ANGULAR MOMENTUM TRANSPORT BY MAGNETIC SHEAR INSTABILITY IN PROTOSTELLAR DISKS

R. Arlt and G. Rüdiger

Astrophysikalisches Institut Potsdam An der Sternwarte 16, D-14482 Potsdam, Germany

Abstract

The efficient transport of angular momentum in a protostellar disk after collapse has been an important issue of star formation for a long time. Turbulent motion in the disk is capable of transporting angular momentum through the disk. The onset of turbulence requires a powerful instability in the roughly Keplerian flow. Among the possible mechanisms of generating this turbulence, the magnetic shear-flow instability appears to be efficient, quick and suitable for a variety of astrophysical surroundings.

We present three-dimensional numerical simulations of disks threaded by a weak magnetic field. The computational domain comprehends the entire disk, azimuthally from 0 to 2π and vertically covering more than a density scale-height. The computations make use of the magnetohydrodynamical computer code ZEUS-3D. The range of magnetic fields necessary for the onset of turbulence is compared with real magnetic field strengths in astrophysical objects. We derive the Shakura-Sunyaev parameter α_{SS} as a measure of the efficiency of angular momentum transport. The simulations have not reached saturation of α_{SS} yet, the current value is $2.5 \cdot 10^{-4}$. Indications for a self-excited dynamo are found which may generate persistent internal magnetic fields providing turbulence over long periods.

Key words: Stars: formation

1. Introduction

The rapid process of star formation requires an efficient transport of angular momentum in the protostellar disk which can be provided by turbulent motion. Searches for instabilities in disks with rotation profiles similar to a Keplerian one unveiled several ways to turbulence being more or less favorable with respect to their prerequisites for the disk configuration. Gravitational instability needs the disk to be either cool or massive, nonlinear and nonaxisymmetric perturbations require a severe additional perturber near the disk, and convection was shown to deliver an inward angular momentum transport (Kley et al. 1993). The requirements for the magnetic shear-flow instability (Balbus & Hawley 1991) do match astrophysical conditions in accretion disks in many configurations. All it needs is a radially decreasing angular velocity and a weak magnetic field threading the rotating object. It can even be shown that the temperature range applicable to the magnetic shear-flow concept is very broad; even very small ionization fractions are sufficient to magnetize a disk in many cases (Balbus & Hawley 1998).

First numerical approaches tackled the local problem; a small box-shaped domain was cut out of the disk, and particular care was taken for the radial boundary conditions which are not simply periodic, but account for the shear due to differential rotation (Hawley et al. 1995).

Linear studies of global configurations of disks threaded by magnetic fields in various directions were carried out. Curry & Pudritz (1995) investigated the stability for vertical and azimuthal fields threading the disk; Rüdiger et al. (1999) particularly addressed the angular momentum transport in their linear study. These investigations are now followed by nonlinear simulations of a compressible fluid with density stratification in global computational domains.

The present computations are not meant as simulations of a star formation process. They focus on the applicability of the magnetic shear-flow instability for an astronomically fast process like the formation of a star. Such global simulations are still a challenge for modern computers and fast algorithms.

2. Simulation outlines

The computations presented here make use of the ZEUS-3D code developed for astrophysical problems of magnetohydrodynamics (Stone & Norman 1992a,b; Stone et al. 1992; Clarke et al. 1994). We use cylindrical coordinates and an extensive computational domain covering radii $r = 5$ to 6, a vertical extension of $h = -0.1$ to $+0.1$, and the full azimuthal range of $\phi = 0$ to 2π. In this approach, we assume an isothermal disk to save computation time on the energy equation. The remaining system for integration is

$$\frac{\partial \rho}{\partial t} + \nabla \cdot (\rho \mathbf{u}) = 0 \quad (1)$$

$$\frac{\partial \rho \mathbf{u}}{\partial t} + \nabla \cdot (\rho \mathbf{u} \cdot \mathbf{u}) = -\nabla p - \rho \nabla \Phi + \mathbf{j} \times \mathbf{B} \quad (2)$$

$$\frac{\partial \mathbf{B}}{\partial t} = \nabla \times (\mathbf{u} \times \mathbf{B}) + \eta \nabla^2 \mathbf{B}, \quad (3)$$

Proc. 33rd ESLAB Symp. *"Star formation from the small to the large scale"*, ESTEC, Noordwijk, 2–5 November 1999 (ESA SP-445, June 2000, F. Favata, A. A. Kaas & A. Wilson eds.)

where ρ, $\mathbf{u}$, and $\mathbf{B}$ are the density, velocity, and magnetic field resp.; p is the pressure ($p \propto \rho$ in our model), Φ is the gravitational potential, $\mathbf{j}$ is the current density, and η is the magnetic diffusivity which is not an original ingredient to the ZEUS code. It is constant in time and space. The gravitational potential is spherically symmetric, whence the z-component of the gravitation is retained within the disk. We therefore obtain a density stratification unlike the computations by Armitage (1998) who omits the z-component of the gravitation and applies periodic boundary conditions for the upper and lower boundaries.

The magnetic field threads the disk vertically with a mere z-component. We tried a homogeneous initial field $B_z(r) = \text{const}$ for the z-boundaries as well as a field

$$B_z(r) = r^{-1} \sin[2\pi(r - r_\mathrm{i})/(r_\mathrm{o} - r_\mathrm{i})] \quad (4)$$

– where r_i and r_o are the inner and outer boundary radii resp. – which has zero total magnetic flux through the $z = \text{const}$ surfaces. The choice of the initial field will have implications for the topology of the field later on. Most of the results presented here were obtained with the second approach except for that in Fig. 1. No magnetic field lines are allowed to penetrate the radial boundary surfaces. Both the radial and the $z = \text{const}$ surfaces are closed for the velocity field. Since we cover the full azimuthal range in ϕ, the boundaries at the $\phi = \text{const}$ surfaces are periodic, naturally. First attempts to account for actual accretion are currently being worked out. The initial velocity field is a merely Keplerian motion following $u_\phi = \sqrt{GM/r}$, where G is the gravitational constant and M is the central mass. The ratio of central mass to the total disk mass is 15:1.

The number of cells in each coordinate direction was $31 \times 61 \times 151$ for the z-, r-, and ϕ-directions. Tests with up to 621 cells in ϕ-direction have been carried out, but the increased computation time does not allow reasonable periods to be covered by the simulation.

3. Results

The non-magnetic Keplerian flow in the disk is found to be locally and linearly stable as expressed by the Rayleigh criterion. The stability of a hydrodynamic Keplerian flow has recently been shown numerically by Hawley et al. (1999). We indeed find that small perturbations in the initial velocity or density fields are damped within a few orbital periods. A test lasting for more than 16 orbital periods proved to converge quickly to a stationary Keplerian solution with an increasing density scale-height H_ρ versus the distance from the central source. The computational domain from $z = -0.1$ to $+0.1$ covers 2.1 scale-heights at the inner radial boundary and 1.5 scale-heights at the outer boundary.

Strong perturbations in the form of a radial wave superposition to the Keplerian rotation profile, such as

$$u_\phi = \sqrt{\frac{GM}{r}} \left[1 + \epsilon \sin\left(2\delta \frac{r}{r_\mathrm{o} - r_\mathrm{i}}\right)\right], \quad (5)$$

where δ represents the wavelength of the perturbation and ϵ its amplitude, can locally violate the Rayleigh criterion. Hydrodynamical tests with such perturbations indeed show global turbulence as soon as the deviations from the Keplerian profile give rise to Rayleigh instability locally. However, low-wavenumber perturbations will be most likely to occur, and it is those which require the largest amplitudes of roughly 10% of the Keplerian velocity.

We now 'switch on' the magnetic field, and we will first determine an instability range for the field strengths from fully magnetohydrodynamical simulations. Comparing the nonlinear results with the linear study in Rüdiger et al. (1999), we normalize the shear flow and the initial magnetic field in terms of a shear-low parameter C_Ω and the Hartmann number Ha. The latter involves the initial field strength $B_z^{(0)}$ for a homogeneous vertical field:

$$\mathrm{Ha} = \frac{B_z^{(0)} H}{\sqrt{4\pi\rho\eta}}. \quad (6)$$

The shear flow parameter

$$C_\Omega = \frac{3\Omega_0 H^2}{2\eta} \quad (7)$$

is here a measure for the magnetic diffusivity only; the rotation law with the angular velocity Ω_0 in the middle of the ring and the disk height H are constants in these simulations. The stability diagram is shown in Fig. 1 and closely resembles the stability curves given in Kitchatinov & Rüdiger (1997) for spherical geometry and Rüdiger et al. (1999) for thin disks. The lower limit for magnetic fields making the flow unstable is controlled by the magnetic diffusivity. There is no lower limit in ideal MHD.

Real physical quantities can be derived if two of the units are fixed; in our case, we choose the distance of the simulated ring from the center and the disk mass. If the ring is placed at 1 au from the center, the instability range converts to magnetic field strengths of 0.4 mGauss to 20 mGauss for $\eta = 0.01$ (in normalized units). A magnetic dipole of a T Tauri star with field strengths near 1 kGauss at the poles will provide a poloidal field of about 10 mGauss through the disk at a distance of 1 au being consistent with the above instability range.

According to the standard model of a turbulent disk according to Shakura & Sunyaev (1973), the stress tensor of velocity and magnetic-field fluctuations,

$$Q_{r\phi} = \left\langle u_r' u_\phi' - \frac{B_r' B_\phi'}{4\pi\rho} \right\rangle, \quad (8)$$

scales as the speed of sound such as

$$Q_{r\phi} = \alpha_\mathrm{SS} c_\mathrm{ac}^2, \quad (9)$$

parameterized by an unknown $\alpha_\mathrm{SS} < 1$. The parameter α_SS actually characterizes a spatial and temporal average of the stress. The present simulations are not evolved to 'stationary' turbulence yet, and we give spatial averages as a function of time below. The sound speed of an isothermal

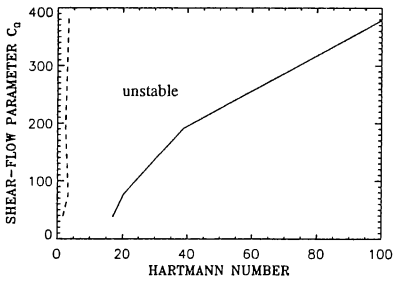

Figure 1. Stability curves for various magnetic diffusivities. The Hartmann number is a measure for the initial vertical field strength, the shear flow parameter measures $1/\eta$.

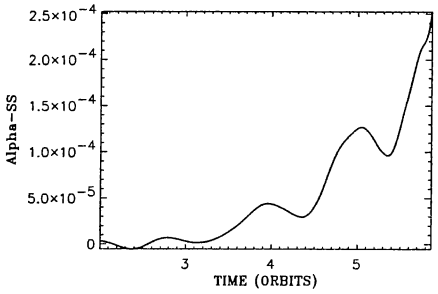

Figure 2. Shakura-Sunyaev-α representing the angular momentum transport in the disk. The graph only shows the period of time after the magnetic field had been switched on.

model is derived from the density scale-height and angular velocity by $c_{ac} = H_\rho \Omega/\sqrt{2}$.

The quick development of appreciable magnitudes of α_{SS} is shown in Fig. 2; the value of α_{SS} increases by almost two orders of magnitudes within less than 4 orbital revolutions. Values between 10^{-3} and 10^{-2} would be required to match the short time-scale of removing the angular momentum of a collapsing cloud from the the inner disk.

At this stage of the simulation, the kinetic part of the stress, the Reynolds stress, dominates the magnetic, the Maxwell stress of the fluctuating quantities. The Reynolds stress exceed the Maxwell stress by several orders of magnitude. Local simulations over long periods of time show the opposite behavior such as for example in Hawley et al. (1995) and Brandenburg et al. (1995). The same holds for the relation of kinetic to magnetic energy as shown in Fig. 3 for the individual components. At least, the energies in all magnetic field components reach very similar orders of magnitude after less than 4 orbits. The energies of the r- and z-components of the velocity remain 4 and 6 orders of magnitude below the Keplerian flow energy.

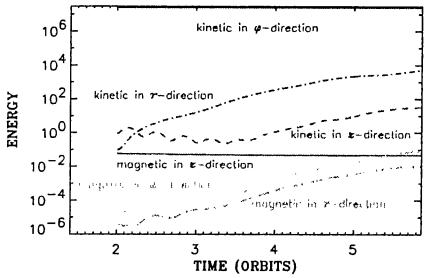

Figure 3. Kinetic and magnetic energies as stored in each of the components.

Figs. 4 and 5 illustrate the development of the azimuthal structure of the disk. The spectral decomposition of each of the magnetic-field components shows some preferred wavelengths in the graph after 2.91 revolutions, which are damped out quickly as can be seen in the 5.87-revolution plot in Fig. 5. The fully developed turbulence in Fig. 5 shows nonaxisymmetric modes of $m = 3$ to $m = 15$ to be dominant in the decomposition of the z- and r-components of the magnetic field.

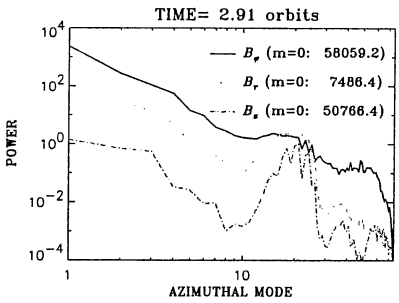

Figure 4. Azimuthal Fourier decomposition of each of the three magnetic-field components after 2.91 orbits of the middle zone of the computational domain.

A typical density snapshot after 5.9 orbital revolutions is shown in Fig. 6. It should be noted that the computational range from $r_i = 5$ to $r_o = 6$ is enlarged in this graph for clearer visibility of the structures. Spiral patterns are visible which are consistent with other experiences in Armitage (1998) for example, and with the azimuthal decomposition given in Fig. 5. The edge-on cross-section in Fig. 7 shows the corresponding 'knots' in the density representing the arms of the spiral pattern.

Rotation, stratification, and turbulence are supposed to be the ingredients for an amplification of large-scale magnetic modes through the so-called α-effect (note the

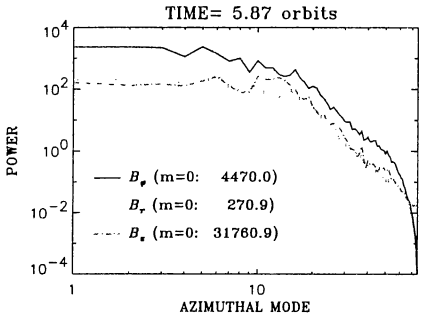

Figure 5. Azimuthal Fourier decomposition of the magnetic-field components after 5.87 orbital periods.

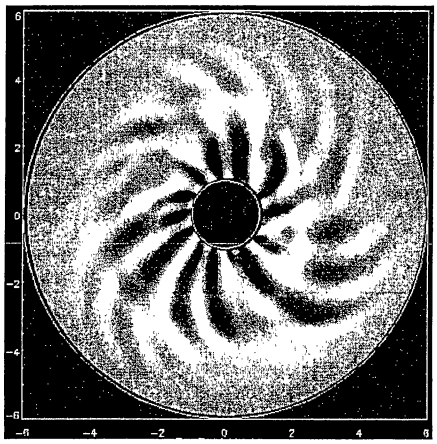

Figure 6. Face-on snapshot of the density in the disk after 5.9 revolutions. The radial scale is enlarged from the original $r_i = 5$ to $r_o = 6$ to a range from 1-6.

difference to α_{SS}), a mean-field approach to explain the generation of global magnetic fields due to dynamo action of appropriate velocity fluctuations. The disk may be able sustain the magnetic fields necessary for the instability on its own through a dynamo. A linear correlation of the ϕ-component of the average electromotive force $\langle u' \times B' \rangle$ to the average magnetic field in that direction, $\langle B_\phi \rangle$, will be a good indication for the validity of this α-concept. Our simulations appear to exhibit a slight correlation, giving a negative slope (that is, a negative dynamo-α) for the northern-hemisphere averages, and a positive slope for the southern-hemisphere averages in agreement with the result of Brandenburg et al. (1995) from a local box simulation.

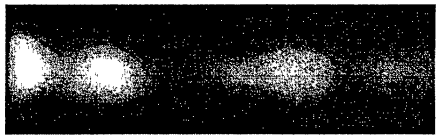

Figure 7. Edge-on snapshot of the density in the disk after 5.9 revolutions. The left edge is the inner boundary at $r_i = 5$, the right edge is at $r_o = 6$. The vertical extent of the graph is 0.2 in these same units.

4. Conclusion

Three-dimensional global simulations have shown, that the magnetic shear-flow instability is a fast mechanism to generate a turbulent flow in a Keplerian disk. The Shakura-Sunyaev parameter α_{SS} increases rapidly during the first revolutions after switching on the magnetic field and. reaches $2.5 \cdot 10^{-4}$ at this stage of the computations, though it is far from saturation. Kinetic energies still dominate the magnetic energies; the Reynolds stress significantly exceeds the Maxwell stress.

Indications for a dynamo action in the disk are found, the corresponding dynamo-α tending to be negative north of the equatorial plane and positive south of the equatorial plane. The generated magnetic fields may maintain the turbulence even if the external field ceases. The strong excitation of low-order azimuthal modes in the magnetic field is another promising fact for dynamo action with respect to the Cowling theorem.

Acknowledgements

We would like to thank D. Elstner from the Astrophysikalisches Institut Potsdam for adding the magnetic diffusivity to the ZEUS-3D code and valuable discussion. R.A. thanks the Deutsche Forschungsgemeinschaft for their support.

References

Armitage, P.J., 1998, ApJ 501, L189
Balbus, S.A., Hawley, J.F., 1991, ApJ 376, 214
Balbus, S.A., Hawley, J.F., 1998, Rev. Mod. Phys. 70, 1
Brandenburg, A., Nordlund, Å., Stein, R.F., 1995, ApJ 446, 741
Clarke D.A., Norman M.L., Fiedler R.A., 1994, ZEUS-3D User Manual, Univ. of Illinois
Curry, C., Pudritz, R.E., 1995, ApJ 453, 697
Hawley, J.F., Balbus, S.A., Winters, W.F., 1999, ApJ 518, 394
Hawley, J.F., Gammie, C.F., Balbus, S.A., 1995, ApJ 440, 742
Kitchatinov, L.L., Rüdiger, G., 1997, MNRAS 286, 757
Kley, W., Papaloizou, J.C.B., Lin, D.N.C., 1993, ApJ 416, 679
Rüdiger, G., Primavera, L., Arlt, R., Elstner, D. 1999, MNRAS 308, 887
Shakura, N.I., Sunyaev, R.A., 1973, A&A 24, 337
Stone J.M., Norman M.L., 1992a, ApJ Suppl. 80, 753
Stone J.M., Norman M.L., 1992b, ApJ Suppl. 80, 791
Stone J.M., Mihalas D., Norman M.L., 1992, ApJ Suppl. 80, 819